Torsional and flexural-torsional buckling of compressed steel members in fire

Luca Possidente[1,2] , Nicola Tondini[1*], Jean-Marc Battini[2]

[1]University of Trento – Department of Civil, Environmental and Mechanical Engineering, Via Mesiano 77, 38123, Trento, Italy

[2]KTH, Royal Institute of Technology - Department of Civil and Architectural Engineering, SE-10044 Stockholm, Sweden.

*Corresponding author: Tel: +39 0461 28 25 36; e-mail: nicola.tondini@unitn.it

Abstract

Torsional and flexural-torsional buckling of compressed steel members are relevant phenomena for monosymmetric and built-up cross-sections frequently employed in bracing systems or in truss structures. Despite the great interest shown by researchers relative to the instability of steel elements in fire, there is a lack of studies on the torsional and flexural-torsional buckling behaviour of steel members in compression at elevated temperature, and no provisions are given in EN 1993-1-2. In this work, a comprehensive numerical investigation of the behaviour of axially compressed angles, Tee and cruciform steel cross-sections at elevated temperature was performed. In this respect, a parametric study was carried out on Class 1 to 3 profiles subjected to uniform temperature distribution. It was found that the buckling curve given in EN 1993-1-2 provides unconservative results for slenderness ranges of practical interest. Improved buckling curves to better predict the behaviour of angles, Tee and cruciform compressed cross-sections at elevated temperature were proposed.

Keywords

Torsional buckling; Flexural-Torsional Buckling; Finite element analysis; Steel structures; Fire; Buckling curve

1. Introduction

The resistance of compressed steel members, usually designated as columns, is influenced by instability phenomena. While members characterised by slender cross-sections may also buckle due to local effects, for more compact sections a global buckling mode, i.e. flexural, torsional or flexural-torsional, governs the behaviour in compression. For typical hot-rolled or welded I or H profiles used as columns in compression, torsional effects are rare, unless flexural buckling around the weak axis is prevented by lateral restraints, as purlins may do in steel industrial halls. However, for angles, Tee and cruciform steel sections, torsional or flexural-torsional buckling usually is the relevant buckling mode. These cross-sections are widely used for bracing systems or for elements in truss structures and angles can be coupled back-to-back to obtain T or cruciform shaped closely built-up sections. Hereafter angles, Tee and cruciform sections are referred to as L, T and X sections respectively. In design practice, the prediction of the behaviour of compressed steel members relies on the buckling curves provided in the Eurocodes, both at ambient [1] and elevated temperature [2]. These curves were first calibrated on H- and I-members and were then extended to other profiles, such as L. In the fire situation many different buckling curves were proposed for compressed steel members. In [3] and [4], Franssen et al. proposed the model for flexural buckling adopted in EN 1993-1-2 [2]. Based on this model, several curves were proposed for other types of instability modes. For instance, in the last years, researchers have put their effort in the investigation of lateral-torsional buckling [5-11] and its interaction with local instabilities [12-14] of steel members subjected to fire. Major findings about the interaction of global and local buckling in hot-rolled Class 4 cross-sections were collected in [15]. Indeed, torsional and flexural-torsional buckling have mainly attracted the interest when the behaviour of cold-formed steel profiles at both ambient and elevated temperatures was concerned [16-21]. For such sections, due to the shape and the small thickness, buckling typically occurs as an interaction of local, distortional and global buckling. Dinis et al. [22] showed such interaction for L, T and X thin-walled columns, beams and beam-columns at ambient temperature. X sections were also investigated at ambient temperature in

[23-25], while laterally restrained I-sections that buckle due to torsional and flexural-torsional deformation were studied in [26]. In addition, a consistent approach of the Ayrton-Perry formulation, on which the European buckling curves are based [1, 2], was proposed for torsional buckling by Chapman et al. [27] and later extended to the general case of beam-columns buckling in [28]. In conclusion, based on the literature review, it is clear that despite the great interest about the instability phenomena of steel structures in fire, there is a paucity of studies devoted to investigate torsional and flexural-torsional buckling at elevated temperatures of hot-rolled and welded steel sections. In this context, the aim of the present work is to fill this gap by numerically investigating the resistance to compression of L, T and X thin-walled steel elements in fire in order to provide improved design buckling curves.

The paper is organised as follows: in Section 2 a brief recall on the buckling of compressed steel members is provided; Section 3 presents the result of a comprehensive parametric analysis on concentrically compressed L, T and X members with Class 1 to 3 subjected to uniform temperature. Numerical analyses were performed by means of beam and shell elements based on a corotational formulation, developed by the authors in [**Errore. L'origine riferimento non è stata trovata.**] and [30]. In Section 4, a new buckling curve model is proposed to account for the buckling behaviour at elevated temperature of L, T and X members and, finally, conclusive remarks are drawn in Section 5.

2. Buckling resistance of compressed steel members in fire

In general, compressed members may buckle due to flexural, torsional or flexural-torsional buckling. For typical H- or I-profiles employed in multi-storey buildings, torsional effects are less likely to occur and compressed columns usually buckle according to a flexural mode around the weak axis. Conversely, torsional or flexural-torsional buckling can be more significant for other cross-section shapes, such as L, T or X sections. In this section, a brief insight into the procedure for the definition of the relevant (lowest) elastic buckling mode and the associated critical load at ambient temperature is provided for monosymmetric, i.e. equal leg L and T sections, and bisymmetric cross-sections (X sections). The general case of sections with no symmetry axes, for instance L sections with unequal legs, was not investigated, because asymmetric profiles are rarely employed in the design practice, as they are usually coupled to obtain monosymmetric profiles, e.g. T sections made of two L profiles. Detailed information about the buckling of monosymmetric and bisymmetric sections can be found in [31, 32]. The derivation of the elastic buckling load at ambient temperature is necessary to the definition of the actual design curve at elevated temperatures (EN 1993-1-2 [2]), which is described in the last part of this section.

2.1. Elastic buckling of monosymmetric and bisymmetric sections

The critical load N_{cr} of a monosymmetric section with symmetry about the y axis (Figures 1a, 1b and 1c) can be defined as the lowest load between the pure flexural critical load $N_{cr,F,z}$ and the flexural-torsional critical load $N_{cr,TF}$.

$$N_{cr} = \min \begin{cases} N_{cr,F,z} = N_{cr,z} \\ N_{cr,TF} = \dfrac{\left(N_{cr,y} + N_{cr,T}\right) - \sqrt{\left(N_{cr,y} + N_{cr,T}\right)^2 - 4N_{cr,y}N_{cr,T}r_0^2/(r_0^2 + y_0^2)}}{2r_0^2/(r_0^2 + y_0^2)} \end{cases} \quad (1)$$

Where $r_0^2 = \left(I_y + I_z\right)/A$ and y_o is the y-coordinate of the centre of torsion (or shear centre) C with respect to the centroid position G. $N_{cr,z}$ and $N_{cr,y}$ are the pure flexural elastic critical loads about the z and y axis respectively and $N_{cr,T}$ is the pure torsional elastic critical load

$$N_{cr,y} = \frac{\pi^2 E I_y}{L_{0y}^2}$$

$$N_{cr,z} = \frac{\pi^2 E I_z}{L_{0z}^2} \quad (2)$$

$$N_{cr,T} = \left(GJ + \frac{\pi^2 E I_w}{L_{0T}^2}\right)\frac{1}{r^2}$$

With $r^2 = \frac{(I_y+I_z)}{A} + y_o$, while L_{0y}, L_{0z} and L_{0T} are the buckling lengths according to the relevant buckling mode. y and z are principal axes, but differently from the Eurocodes nomenclature, y is not necessarily the strong axis. In fact, for equal leg L profiles and T sections obtained by coupling two of those L profiles (see Figure 1a and 1b), y is always the strong axis. However, when two L profiles with unequal legs were coupled, the strong axis of the T section became the z axis, as shown in Figure 1c.

In bisymmetric sections the centroid and the centre of torsion coincide and thus, $y_o = z_o = 0$ (see Figure 1d). Interaction between the different buckling modes disappears and the critical load N_{cr} is simply the lowest between the pure flexural and pure torsional buckling loads given in Eq. (2).

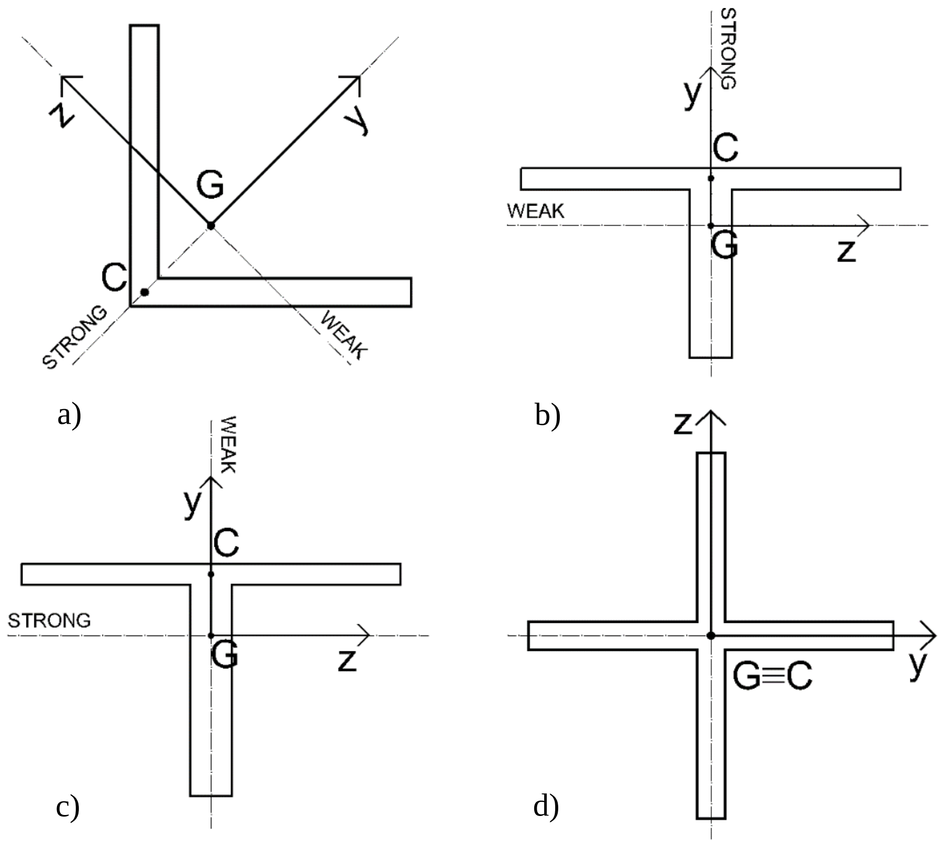

Fig. 1. Analysed sections a) L section, b) T section built up with 2 equal leg L; c) T section built up with 2 unequal leg L; d) X section

2.2. Design provisions for members in fire

Since an improved buckling curve will be proposed in Section 4, a brief review of the procedure for the definition of the design buckling resistance of compressed steel members in fire $N_{b,fi,t,Rd}$ as given in EN 1993-1-2 [2] is here provided. The resistance of members of Class 1, Class 2 or Class 3 cross-sections with uniform steel temperature θ_a is determined from:

$$N_{b,fi,t,Rd} = \chi_{fi} A k_{y,\theta} f_y / \gamma_{M,fi} \tag{3}$$

where $\gamma_{M,fi}$ is the safety factor for the fire design situation, A is the area of the cross-section, $k_{y,\theta}$ is the reduction factor for the yield strength of steel at temperature θ_a and f_y is the yield strength at ambient temperature. The formulation consists in the reduction of the cross-sectional compression capacity by the flexural buckling coefficient in the fire design situation χ_{fi}. This coefficient should be determined according to the following equation:

$$\chi_{fi} = \frac{1}{\varphi_\theta + \sqrt{{\varphi_\theta}^2 - {\bar{\lambda}_\theta}^2}} \tag{4}$$

with

$$\varphi_\theta = \frac{1}{2}\left[1 + \eta_{EC3.1-2} + {\bar{\lambda}_\theta}^2\right] \tag{5}$$

The generalised imperfection factor $\eta_{EC3.1-2}$ is defined as

$$\eta_{EC3.1-2} = \alpha \bar{\lambda}_\theta \tag{6}$$

α is the imperfection factor, which depends on the yield strength f_y expressed in MPa

$$\alpha = \beta\sqrt{235/f_y}; \qquad \beta = 0.65 \tag{7}$$

The non-dimensional slenderness $\bar{\lambda}_\theta$ at the temperature θ_a, is given by:

$$\bar{\lambda}_\theta = \bar{\lambda}\left[k_{y,\theta}/k_{E,\theta}\right]^{0.5} \tag{8}$$

where $k_{y,\theta}$ and $k_{E,\theta}$ are the reduction factors for the yield strength and Young's modulus at temperature θ_a, respectively, and $\bar{\lambda}$ is the non-dimensional slenderness at ambient temperature. No further information about the definition of $\bar{\lambda}$ is given in this code. Moreover, since χ_{fi} is defined as the smaller between the flexural buckling coefficients $\chi_{y,fi}$ and $\chi_{z,fi}$, it seems that no particular attention has been given to possible flexural-torsional behaviour. However, EN 1993-1-1 [1] prescribes that at ambient temperature the reduction factor should be defined according to the slenderness associated with the lowest relevant buckling mode, as shown in Eq. (9). In fact, for Class 1, 2 and 3 cross-sections it reads:

$$\bar{\lambda} = \bar{\lambda}_{cr} = \sqrt{\frac{Af_y}{N_{cr}}} \tag{9}$$

where N_{cr} is the lowest elastic critical load at ambient temperature, as defined in Eq. (1). Hence, it seems reasonable to employ a similar method in the fire situation and to define more in general χ_{fi} as a function of the relevant buckling mode at elevated temperature, as presented in Section 4.

3. Parametric analysis

In order to check whether the EN 1993-1-2 buckling curve provides accurate and safe predictions of concentrically compressed members subjected to fire that may be sensitive to torsional or flexural-torsional buckling, a large number of Finite Element Analysis (FEA) were carried out. In particular, more than 23500 geometrically and materially imperfect nonlinear analyses (GMNIA) were performed on columns, axially compressed through the centroid of the cross section, with different length and temperature by means of 3D beam and shell elements. The finite elements employed in this paper are based on a corotational formulation and are suitable for the analysis of steel structures in fire conditions. Their features and capabilities, as well as their validation against well-known commercial software, are detailed in [29, 30]. In [29] it was shown that, differently from the beam elements used in commercial software like ABAQUS and SAFIR, the beam elements employed in this paper properly allow for torsional behaviour at elevated temperature. Thus, they are particularly suited for the analysis of structural elements with open cross-sections subjected to torsional actions such as torsion, torsional buckling, flexural-torsional buckling and lateral-torsional buckling.

Further details about the employed finite elements can be found in [29, 30]. The columns were subjected to uniform temperature distributions from 400°C to 800°C, as similarly to columns that buckle flexurally [3], this is the most relevant temperature range for practical cases. Hence, columns subjected to five different uniform temperatures were studied (400°C, 500°C, 600°C, 700°C, 800°C): for each temperature about 4700 columns were analysed. In order to investigate steel columns of practical interest, the members had a minimum length of at least 3 times the largest cross-section dimension.

45 different equal leg L profiles of commercial dimensions were studied. 68 T sections and 45 X sections were defined by coupling 2 and 4 L sections, respectively. Sectional dimensions of the investigated columns are reported in Tables 1-3 for all section types. In the case of closely built-up members, in which L sections are connected through packing plates or for star-battened angles, members can be checked for buckling as single integral members if the spacing of the connections is short enough [1]. As performed by other authors [22-25], the behaviour of coupled members considered as single and integral, leads to meaningful predictions of the buckling modes. Nevertheless, it is clear that a more refined numerical investigation could be performed accounting for the connecting plates or battens in the models. In the parametric analysis, the cross-sections were of Class 1, Class 2 or Class 3. The classification in fire situation was performed according to EN 1993-1-2 [2]. The class of each investigated cross-section is provided in Tables 1-3. Since closely built-up sections are usually connected at discrete points along the member length, it was decided to conservatively classify the T and X cross sections based on the classification of the single angular of which they are composed. It has to be noted that in particular for single angles with equal legs in pure compression, due to the class limits given in the Eurocode, the cross sections are essentially either of Class 1 or of Class 4. Since the behaviour of Class 4 cross-sections is affected by local buckling that occurs before the attainment of yield stress in one or more parts of the cross-section [1], they were not studied and a separate investigation would be necessary. Therefore, most of the cross sections were of Class 1. Moreover, commercial L profiles with

unequal legs were mainly in Class 4 and thus, less profiles were available for numerical investigation of T section made of these sections.

Table 1. List of the cross-section dimensions for L and X profiles

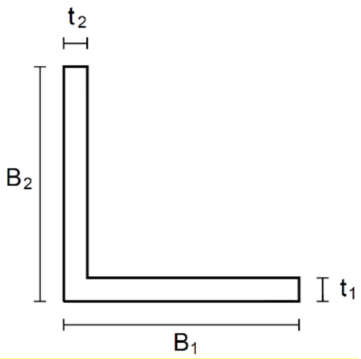

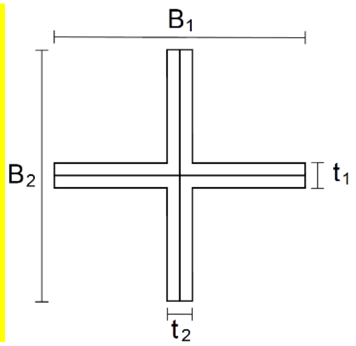

Section	L section B_1 (=B_2) [m]	L section t_1 (=t_2) [m]	L section B_1/t_1	X section B_1 (=B_2) [m]	X section t_1 (=t_2) [m]	X section B_1/t_1	S235	S275	S355
	0.050	0.009	5.56	0.100	0.018	5.56		$+^1$	$*^1$
	0.090	0.016	5.63	0.180	0.032	5.63	$\square^1$	$+^1$	$*^1$
	0.065	0.011	5.91	0.130	0.022	5.91			$*^1$
	0.060	0.010	6.00	0.120	0.020	6.00		$+^1$	$*^1$
	0.100	0.016	6.25	0.200	0.032	6.25	$\square^1$	$+^1$	$*^1$
	0.045	0.007	6.43	0.090	0.014	6.43		$+^1$	$*^1$
	0.065	0.010	6.50	0.130	0.020	6.50		$+^1$	$*^1$
	0.100	0.015	6.67	0.200	0.030	6.67	$\square^1$	$+^1$	$*^1$
	0.200	0.028	7.14	0.400	0.056	7.14		$+^1$	$*^1$
	0.250	0.034	7.35	0.500	0.068	7.35		$+^1$	$*^1$
	0.150	0.020	7.50	0.300	0.040	7.50	$\square^1$		$*^1$
	0.250	0.033	7.58	0.500	0.066	7.58		$+^1$	$*^1$
	0.200	0.026	7.69	0.400	0.052	7.69	$\square^1$	$+^1$	$*^1$
	0.070	0.009	7.78	0.140	0.018	7.78		$+^1$	$*^1$
	0.250	0.032	7.81	0.500	0.064	7.81			$*^1$
	0.120	0.015	8.00	0.240	0.030	8.00	$\square^1$	$+^1$	
	0.150	0.018	8.33	0.300	0.036	8.33	$\square^1$	$+^1$	
	0.140	0.016	8.75	0.280	0.032	8.75	$\square^1$	$+^1$	
	0.300	0.033	9.09	0.600	0.066	9.09	$\square^1$		
	0.110	0.012	9.17	0.220	0.024	9.17	$\square^1$		
	0.120	0.013	9.23	0.240	0.026	9.23	$\square^1$		
	0.250	0.027	9.26	0.500	0.054	9.26	$\square^1$		
	0.140	0.015	9.33	0.280	0.030	9.33			
	0.300	0.032	9.38	0.600	0.064	9.38	$\square^2$		
	0.160	0.017	9.41	0.320	0.034	9.41	$\square^1$		
	0.180	0.019	9.47	0.360	0.038	9.47	$\square^1$		

Superscript = Class at elevated temperature [2]

Table 2. List of the cross-section dimensions for T profiles (coupled equal leg L profiles)

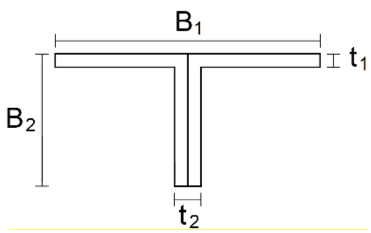

Section	B_1 [m]	B_2 [m]	t_1 [m]	t_2 [m]	B_1/t_1	B_2/t_2	S 235	S 275	S 355
	0.100	0.050	0.009	0.018	11.11	2.78		$+^1$	$*^1$
	0.180	0.090	0.016	0.032	11.25	2.81	$\square^1$	$+^1$	$*^1$
	0.130	0.065	0.011	0.022	11.82	2.95			$*^1$
	0.120	0.060	0.010	0.020	12.00	3.00		$+^1$	$*^1$
	0.200	0.100	0.016	0.032	12.50	3.13	$\square^1$	$+^1$	$*^1$
	0.090	0.045	0.007	0.014	12.86	3.21		$+^1$	$*^1$
	0.130	0.065	0.010	0.020	13.00	3.25		$+^1$	$*^1$
	0.200	0.100	0.015	0.030	13.33	3.33	$\square^1$	$+^1$	$*^1$
	0.400	0.200	0.028	0.056	14.29	3.57		$+^1$	$*^1$
	0.500	0.250	0.034	0.068	14.71	3.68		$+^1$	$*^1$

Section	B_1 [m]	B_2 [m]	t_1 [m]	t_2 [m]	B_1/t_1	B_2/t_2	S 235	S 275	S 355
	0.300	0.150	0.020	0.040	15.00	3.75	$\square^{1}$		$*^{1}$
	0.500	0.250	0.033	0.066	15.15	3.79		$+^{1}$	$*^{1}$
	0.400	0.200	0.026	0.052	15.38	3.85	$\square^{1}$	$+^{1}$	$*^{1}$
	0.140	0.070	0.009	0.018	15.56	3.89		$+^{1}$	$*^{1}$
	0.500	0.250	0.032	0.064	15.63	3.91			$*^{1}$
	0.240	0.120	0.015	0.030	16.00	4.00	$\square^{1}$	$+^{1}$	
	0.300	0.150	0.018	0.036	16.67	4.17	$\square^{1}$	$+^{1}$	
	0.280	0.140	0.016	0.032	17.50	4.38	$\square^{1}$	$+^{1}$	
	0.600	0.300	0.033	0.066	18.18	4.55	$\square^{1}$		
	0.220	0.110	0.012	0.024	18.33	4.58	$\square^{1}$		
	0.240	0.120	0.013	0.026	18.46	4.62	$\square^{1}$		
	0.500	0.250	0.027	0.054	18.52	4.63	$\square^{1}$		
	0.280	0.140	0.015	0.030	18.67	4.67			
	0.600	0.300	0.032	0.064	18.75	4.69	$\square^{2}$		
	0.320	0.160	0.017	0.034	18.82	4.71	$\square^{1}$		
	0.360	0.180	0.019	0.038	18.95	4.74	$\square^{1}$		
Superscript = Class at elevated temperature [2]									

Table 3. List of the cross-section dimensions for T profiles (coupled unequal leg L profiles)

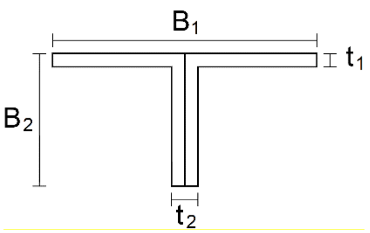

Section	B_1 [m]	B_2 [m]	t_1 [m]	t_2 [m]	B_1/t_1	B_2/t_2	S 235	S 275	S 355
	0.100	0.130	0.009	0.018	11.11	7.22	$\square^{3}$		
	0.100	0.130	0.010	0.020	10.00	6.50	$\square^{2}$	$+^{3}$	
	0.100	0.130	0.012	0.024	8.33	5.42	$\square^{1}$	$+^{1}$	$*^{2}$
	0.110	0.140	0.010	0.020	11.00	7.00	$\square^{3}$	$+^{3}$	
	0.110	0.140	0.012	0.024	9.17	5.83	$\square^{1}$	$+^{2}$	$*^{3}$
	0.120	0.160	0.012	0.024	10.00	6.67	$\square^{2}$	$+^{3}$	
	0.130	0.180	0.012	0.024	10.83	7.50	$\square^{3}$		
	0.130	0.180	0.014	0.028	9.29	6.43	$\square^{1}$	$+^{2}$	$*^{3}$
	0.140	0.180	0.012	0.024	11.67	7.50	$\square^{3}$		
	0.140	0.180	0.014	0.028	10.00	6.43	$\square^{2}$	$+^{3}$	
	0.150	0.200	0.014	0.028	10.71	7.14	$\square^{3}$	$+^{3}$	
	0.200	0.200	0.016	0.032	12.50	6.25	$\square^{3}$		
Superscript = Class at elevated temperature [2]									

3.1. Numerical model

The material nonlinearity was introduced with the nonlinear stress-strain constitutive law of steel at elevated temperatures, while residual stresses were deemed negligible. The latter assumption was extensively investigated by many authors and residual stresses were always found to have no significant effects on the resistance of steel members in fire [3,11,20,33,34,35]. In fact, residual stresses at ambient temperature influence the plate load-bearing capacity but at elevated temperatures a relaxation effect of initial residual stresses is likely to occur owing to the steel temperature increase [33,35]. The steel elasto-plastic isotropic behaviour was based on the Von

Mises yield function and on the uniaxial stress-strain relationship provided by the EN 1993-1-2 [2]: Young's modulus at ambient temperature equal to 210 GPa, Poisson ratio equal to 0.3 and three different steel grades, namely S235, S275, S355 were adopted. For each column initial geometric imperfections were defined according to the buckling mode obtained by a linear eigenvalue buckling analysis. The imperfections were scaled in order to obtain a maximum nodal displacement along the column of 1/1000 of the length. Note that when a pure torsional imperfection is introduced in X sections the maximum nodal displacement is the displacement induced by rotation ϑ at the end node of one of the flanges (see Figure 2a).

Beam finite elements developed in [**Errore. L'origine riferimento non è stata trovata.**] were employed for the monosymmetric sections, whereas for the X section, due to the nature of its buckling behaviour, the shell element proposed in [30] was used in the numerical simulation. Indeed, in beam analyses the introduction of imperfections associated to a pure torsional buckling of a bisymmetric section would results in no displacement of the centroid of the section. Thus, the configuration of the columns would essentially remain undisturbed. This is not the case of shell analyses, in which not only the centroid, but also the nodes that define the section can be displaced, allowing for proper representation of torsion (see Figure 2a). Nevertheless, beam elements were used for the monosymmetric cross-sections as they allow for faster analyses and an easier definition of the boundary conditions. In these analyses simply-supported conditions were employed. The rotation along the longitudinal axis was blocked. In shell element-based models, simply supported conditions are not straightforward to apply and the investigation of clamped columns was instead preferred. The axial displacement was free on the loaded side and fixed on the opposite one. The axial load was applied to the centroid and uniform axial displacement was guaranteed on the loaded side by master-slave constraints. Convergence investigation proved that 30 elements were sufficient for accurate solutions in beam analyses, while the mesh varied with the length of the columns in the shell-based simulations. The depth-to-width ratio of the shell elements was kept constant and close to 1, as for this ratio the employed triangle elements have the best performance. 7 nodes in each dimension of the section were always used. The typical deformed configuration of half of the member associated with a pure torsional and a pure flexural buckling mode for a X section with B_1=0.3m and t_1=0.04m are depicted in Figure 2b and Figure 2c respectively.

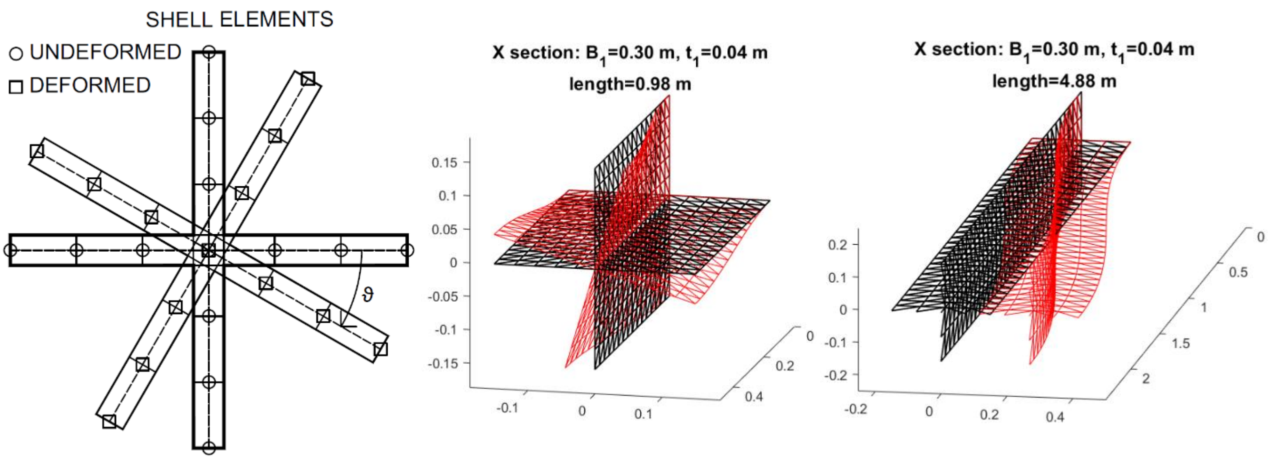

Fig. 2. Shell model for X sections: a) imperfection for the torsional mode; b) deformed shape of half of the member due to torsional buckling mode; c) deformed shape of half of the member due to flexural buckling mode.

3.2. Validation of the numerical model

A preliminary analysis was carried out to validate the numerical model, as proposed in [35]. The numerical results for the flexural buckling of an IPE300 S235 steel column about the strong axis were compared to the relevant buckling curve given in EN 1993-1-1 [1]. The numerical analysis was performed on simply supported columns by means of the beam finite element. Flexural buckling about the weak axis was prevented by restraining the out-of-plane displacements at all the nodes along the beam, as shown in Figure 3a. Columns of different lengths (and thus in turn slenderness $\bar{\lambda}$) were tested by applying an increasing axial load and measuring the load at failure. As suggested by Jönsson and Stan in [36], in order to reproduce the European buckling curves, finite element analysis may be performed with equivalent column bow imperfections extracted directly from the Ayrton-Perry formulation. As a result, being the generalised imperfection factor η in the analytical Ayrton-Perry approach for the derivation of the buckling curves defined as $\eta = e/k$, it turns out that for the generalised imperfection factor proposed in EN 1993-1-1 [1] one gets

$$\eta_{EC3.1-1} = \alpha(\bar{\lambda} - 0.2) = e/k \tag{10}$$

Where $\bar{\lambda}$ is the non-dimensional slenderness as defined in Eq. (9), e is the eccentricity of the column and k is kernel radius. The latter is the ratio between the relevant section modulus W of the section, i.e. the one about the strong axis in this case, and the cross-section area A ($k = W/A$). It follows that introducing an imperfection e derived from Eq. (10) a good numerical model should give results in very good agreement with the Eurocode buckling curve. Thus, the geometric imperfection introduced in the model was defined as follows

$$e = \alpha k(\bar{\lambda} - 0.2) \tag{11}$$

Numerical analysis and the buckling curve a are compared in Figure 3b, where the ratio between the failure load N and the yield load N_{yield} is plotted against the non-dimensional slenderness $\bar{\lambda}$. From Figure 3b it is possible to observe a good agreement between design predictions and numerical outcomes. The fact that numerical results are almost superimposed to the buckling curve from EN 1993-1-1 proves the reliability of the implemented model.

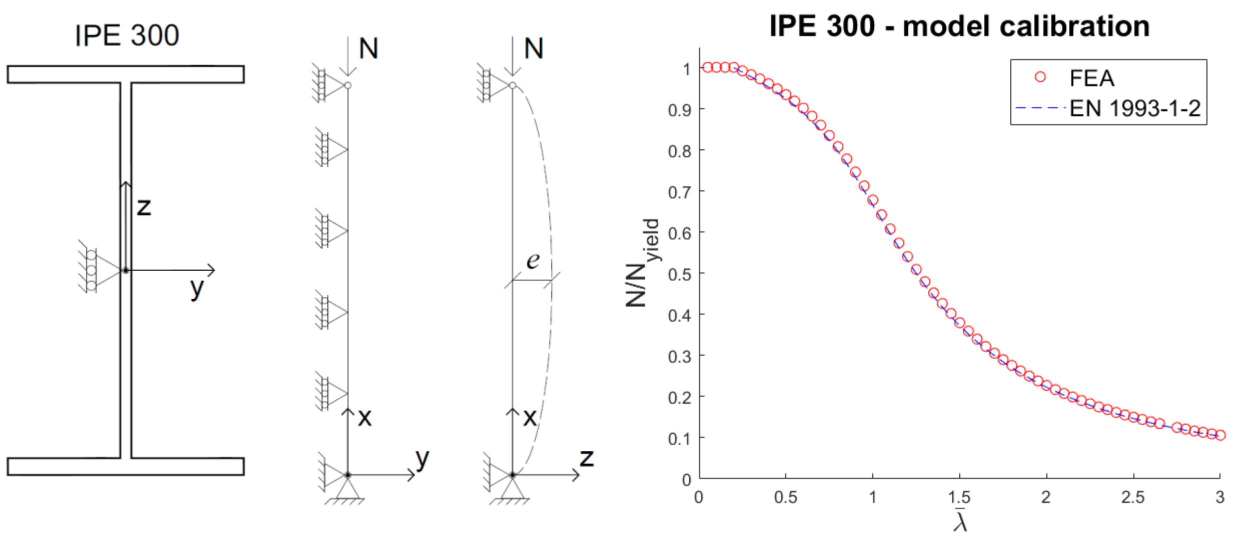

a) b)

Fig. 3. Model validation: a) IPE300 constraints; b) Numerical results vs. design curve predictions

As no experimental tests are available in literature, a further numerical validation is here presented to check the ability of the developed models to well capture flexural-torsional buckling. In this respect, the behaviour of a compressed T 300x150x20x40 section (see Table 2) at 600°C was investigated by means of both the beam and shell finite elements employed in this work. The column was clamped at the ends and the length was chosen so that the column was sensitive to flexural-torsional buckling, i.e. L=1.67 m. In fact, linear buckling analysis identified flexural-torsional buckling as the lowest buckling mode for both shell and beam models, as shown in Figure 4a. The associated critical buckling loads were $N_{cr,BEAM}$ = 12150 kN and $N_{cr,SHELL}$= 12550 kN for the beam and the shell models, respectively, which means a difference of 3.2%. Once identified, the first buckling mode shape was scaled and introduced as initial imperfection in the numerical models. A constant and uniform temperature of 600°C was applied to the column and the compressive load N was then increased at each step of the analysis. Results in terms of the ratio between the applied axial load N and the yield load $N_{yield} = Ak_{y,600°C}f_y$ are given in Figure 4b as a function of the axial displacement of the loaded node. For comparison purposes, the outcomes of the same analysis performed with a shell model developed in SAFIR [37] are also shown in Figure 4b. The three analyses are in excellent agreement and an almost identical load level with a maximum difference of 3.7% was reached.

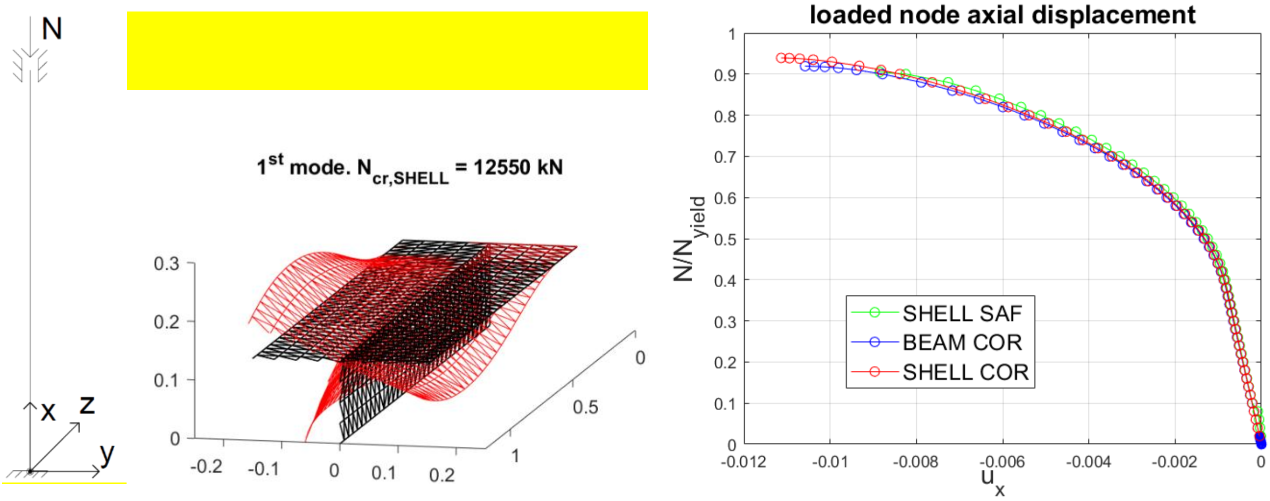

Fig. 4. a) T 300x150x20x40 constraints and lowest buckling mode; b) Load vs axial displacement of the loaded node

3.3. Numerical results

The results of the parametric analysis for the 4 different section shapes are shown in Figure 5 and compared with the EN 1993-1-2 [2] buckling curve at elevated temperature. In Figure 5 each single graph shows the results obtained through non-linear FE analysis by varying the length of the members defined in Tables 1-3. The numerical failure load N is expressed with respect to the yield load at elevated temperature $N_{yield} = Ak_{y,\theta}f_y$, while the slenderness at elevated temperature $\bar{\lambda}_\theta$ (see Eq. (8)) of the investigated columns was defined according to the relevant buckling mode. As the slenderness affects the distribution of the plotted numerical data, the geometrical properties used for its definition should be carefully evaluated. In the beam analysis the Saint-Venant torsional constant J and the warping torsional constant I_w were determined by means of finite element numerical analysis. These two numerical quantities may differ from the ones obtained through the analytical equations [38,39] typically employed in the design practice. As one of the purposes of this work is to provide buckling curves that could be used in design practice, the non-dimensional slenderness $\bar{\lambda}_\theta$ was determined according to the geometrical properties derived analytically.

A brief separate discussion is addressed for the X sections studied by means of shell elements. Buckling occurred in its pure flexural form for almost all the numerical results in Figure 5. Additional analyses were performed for stockier columns, which buckled torsionally, but the results associated to these columns occurred for loads higher than the yield load ($N > N_{yield}$). Several researches showed that columns may attain failure loads exceeding the yield load when shell elements are employed [12-14, 21]. However, such results were not considered as they would imply buckling coefficients $\chi_{fi} > 1$, whereas χ_{fi} should never exceed the value of 1. Nevertheless, even though the data reported in Figure 5 for X sections are mainly associated to pure flexural buckling, a new buckling curve was proposed in Section 4, as the predictions from the EN 1993-1-2 design curve do not accurately represent the numerical observations.

It can be noted that columns with $\bar{\lambda}_\theta \geq 0.7$ consisting of L and T profiles are not particularly sensitive to torsional effects and mainly buckle according to a flexural mode. In the $0.25 \leq \bar{\lambda}_\theta < 0.7$ range torsional effects are more important and numerical results are more scattered, especially for L sections. The appearance of scattered data is mainly related to the use of analytical quantities in the definition of the non-dimensional slenderness $\bar{\lambda}_\theta$. In fact, for L, T and X sections the analytical warping torsional constant I_w is zero and the pure torsional buckling load $N_{cr,T}$ does not vary with the length of the column (see Eq.(2)). This load affects the value of $\bar{\lambda}_\theta$ by means of Eq.(1), (8) and (9). Thus, the more the column length decreases, the more the torsional effects become significant, the lesser $\bar{\lambda}_\theta$ varies with the length of the column and numerical data are consequently not well distributed along the abscissa. In addition, numerical results are affected by the B/t ratio, as shown in Figure 6b, and cannot be easily represented by buckling curves that do not account for the influence of this parameter. Pure flexural buckling governed the behaviour of X members in the whole plotted slenderness range characterised by $\bar{\lambda}_\theta > 0.20$ and numerical outcomes are less scattered.

When numerical data are compared to the actual design curve, a few common traits can be identified. As expected, good predictions are obtained for slender columns with $\bar{\lambda}_\theta \geq 1.5$, when flexural buckling governs the failure of all the section types. Nevertheless, the buckling curve from EN 1993-1-2 provides non-conservative results for a large slenderness range of practical interest. Indeed, by decreasing the slenderness, the resistance to compression is overpredicted, while at about $\bar{\lambda}_\theta = 0.5$ predictions are both safe and unsafe. This is the case in particular of L and T profiles, for which scattered numerical data appear due to the definition of the non-dimensional slenderness $\bar{\lambda}_\theta$, as explained before. For very stocky columns ($\bar{\lambda}_\theta < 0.5$) predictions are mainly overconservative for L, T and X sections. Thus, the introduction of improved buckling curves to better predict the behaviour of L, T and X compressed cross-sections at elevated temperature would be beneficial.

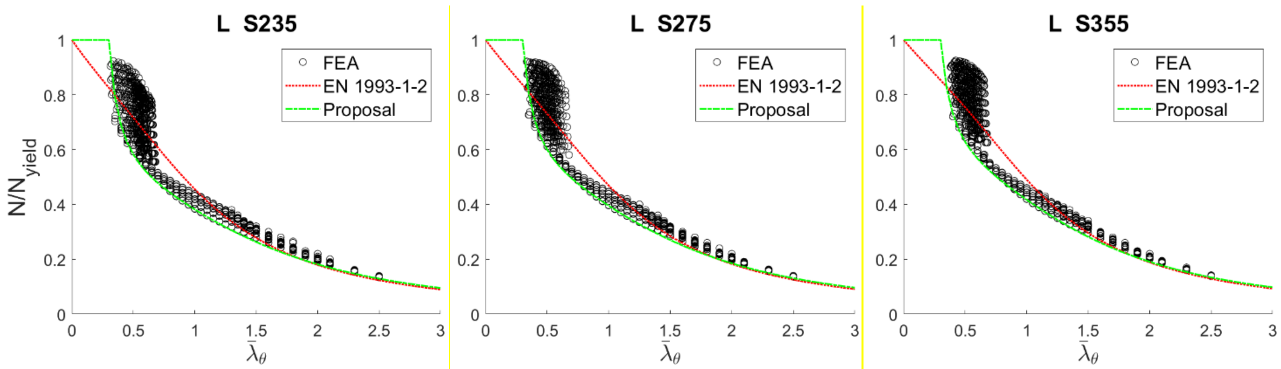

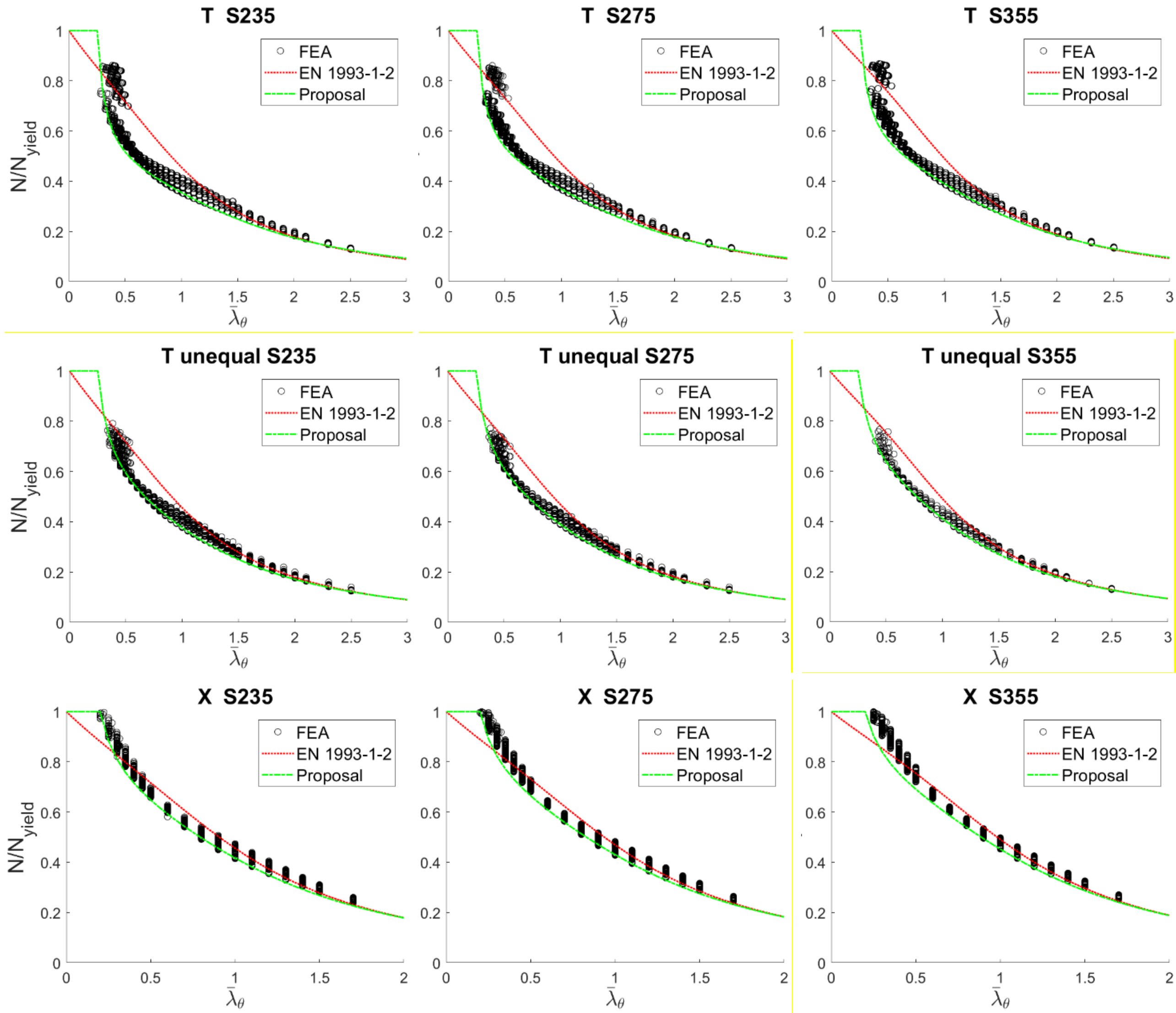

Fig. 5. Buckling curves for S235, S275 and S355

All subfigures of Figure 5 include the effects of different temperatures and of the B/t ratio that deserve a deeper description. The numerical results obtained for each investigated temperature are shown in Figure 6a for an L150x150x20x20 (B/t =7.5) section with S355 steel grade. Similar observations can be made for all the cross-sections and steel grades. Though the resistance at elevated temperature is significantly lower than the one at ambient temperature, there is no big variation in the 400°C-800°C range. For columns subjected to significant torsional effects ($\bar{\lambda}_\theta <$ 0.7), the result variation is larger. Similar observations can be made for the T cross-sections. Analogously, the influence of the B/t ratio is illustrated in Figure 6b, where the failure loads of all the investigated L sections are presented for temperature equal to 400°C and steel grade equal to 355MPa. It can be observed that the B/t ratio has no influence on the results until torsional effects are significant, i.e. $\bar{\lambda}_\theta < 0.7$. Hence, for very stocky columns, predictions obtained from a single buckling curve regardless of the temperature and of the B/t ratio are less accurate for $\bar{\lambda}_\theta < 0.7$. However, it was decided to propose one simple model of buckling curve that provides safe and reasonable accurate predictions. It is worth to point out that the variation of results for $\bar{\lambda}_\theta < 0.7$ was considerably reduced in the second model when the flexural slenderness at elevated temperature is used, as described in Section 4.2.

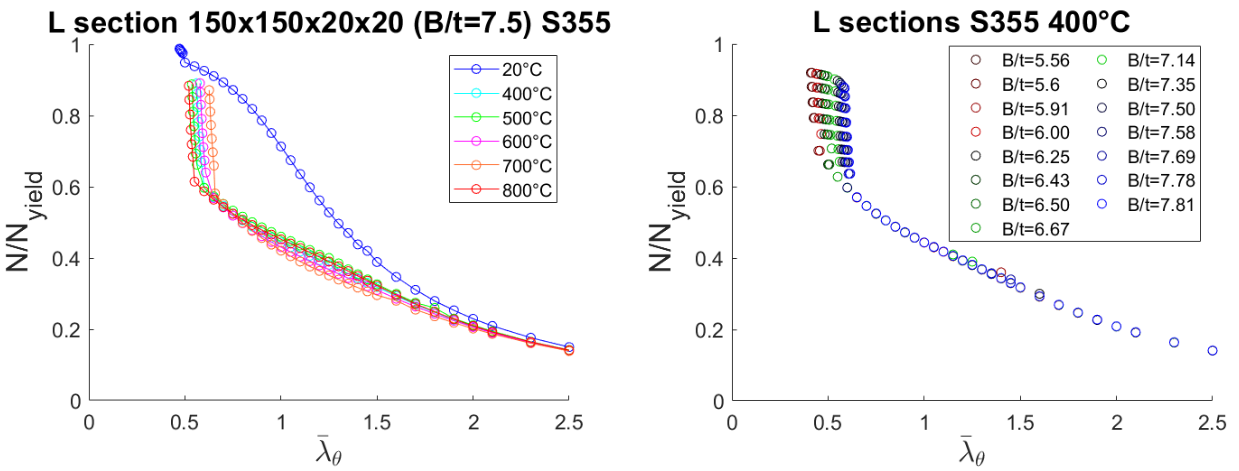

Fig. 6 a) Influence of temperature on numerical results for an L150x150x20x20 S355 steel section; b) Influence of the B/t ratio on numerical results for L S355 steel section at 400°C

4. Buckling curve proposal

The procedure provided in EN 1993-1-2 [2] was modified based on the results from the parametric analysis. Both the procedures at ambient [1] and at elevated temperature [2] are derived from the same equations and differ only in the definition of the generalised imperfection factor η. At elevated temperature $\eta_{EC3.1-2} = \alpha\bar{\lambda}_\theta$ (see Eq. (5)), while at ambient temperature a plateau representing the evolution of the buckling reduction factor χ is introduced for non-dimensional slenderness values $\bar{\lambda} \leq 0.2$, by defining $\eta_{EC3.1-1}$ as $\alpha(\bar{\lambda}_\theta - \bar{\lambda}_0)$ and $\bar{\lambda}_0 = 0.2$. With non-dimensional slenderness values $\bar{\lambda} \leq 0.2$, χ at ambient temperature is equal to 1. Different imperfection factors α are provided at ambient temperature according to the shape, the buckling mode and the steel grade of the member. In a similar fashion, the proposed model is in line with the formulation of buckling curves from [1] and [2] and only the generalised imperfection factor η in Eq. (5) was modified as follows:

$$\eta_{PROP} = \frac{\alpha}{\bar{\lambda}_\theta{}^{\gamma}}\left(\bar{\lambda}_\theta - \frac{\bar{\lambda}_0^2}{\bar{\lambda}_\theta}\right) \tag{12}$$

As the imperfection factor α is defined according to Eq. (7), only 3 parameters, namely β, γ and $\bar{\lambda}_0$ are needed for the complete definition of the buckling curve, i.e. the evolution of χ_{fi} with $\bar{\lambda}_\theta$. $\bar{\lambda}_0$ represents the non-dimensional slenderness limit for the plateau. Thus, Eq. (4) should be replaced by

$$\begin{aligned} \chi_{fi} &= 1 & \bar{\lambda}_\theta &\leq \bar{\lambda}_0 \\ \chi_{fi} &= \frac{1}{\varphi_\theta + \sqrt{\varphi_\theta{}^2 - \bar{\lambda}_\theta{}^2}} & \bar{\lambda}_\theta &> \bar{\lambda}_0 \end{aligned} \tag{13}$$

The values of β, γ and $\bar{\lambda}_0$ associated with the proposed curves shown in Figure 5 are given in Table 4. The calibration of such parameters was performed by comparing the predictions with the results of the parametric analysis, as illustrated in Figure 5 and Figure 7. The aim was to propose design buckling curves on the safe side and easy to apply. In addition, curves associated with normal distributions with small standard deviations and high probabilities of non-exceedance of the safe-unsafe limit were preferred, as depicted in Figure 8. Several combinations of parameters were tested until the optimal agreement between the proposed design curve and the numerical outcomes was obtained.

Table 4. Parameter values for the proposed buckling curve

	L	T	T (unequal)	X
β	1.10	1.25	1.10	0.85
γ	0.80	0.80	0.50	0.35
$\bar{\lambda}_0$	0.30	0.25	0.25	0.20

4.1. Buckling curves comparison

Both the EN 1993-1-2 [2] and the proposed design buckling curves are depicted in Figure 5. The EN 1993-1-2 design buckling curve is not well-suited for the context of flexural-torsional buckling. The buckling coefficient χ_{fi} is overestimated for a medium slenderness range, while the absence of a plateau leads to over-conservative predictions for very stocky columns. The proposal represents more accurately the buckling resistance of compression members that are sensitive to torsional and flexural-torsional buckling. The degree of safety of the buckling curves was assessed by comparison with the results from numerical simulation. In detail, the failure loads of the buckling curves were calculated for each non-dimensional slenderness $\bar{\lambda}_\theta$ employed in the numerical analyses and were plotted against the associated numerical failure load N_{FEA} (Figure 7). The numerical (N_{FEA}) and the failure loads computed with the proposed buckling curve and the EN 1993-1-2 buckling curve (N) were normalised by means of the yield load N_{yield}. In Figure 7, the safe-unsafe limit is identified by the first quadrant bisector line ($N = N_{FEA}$). The EN 1993-1-2 design buckling curve overestimates the numerical failure load of L and T sections in the range $0.3 < N_{FEA}/N_{yield} < 0.7$. Predictions of the load-bearing capacity attain values significantly higher than the ones from the numerical simulation (>10%). For higher values of N_{FEA}/N_{yield}, the EN 1993-1-2 buckling curve is safer and is conservative from values $N_{FEA}/N_{yield} > 0.8$. In case of X sections, the EN 1993-1-2 buckling curve results are approximately in the $\pm 10\%$ range. Nevertheless, the proposed buckling curve is safer than the Eurocode one. The predictions are much better distributed in the safe range between -10% and 0%, in particular for observations associated with flexural buckling. When torsional effects are more significant, the proposed curve is still safe, but the predictions are spread on a large range of values and might significantly underestimate the compression resistance. Excellent agreement was found when the proposed curve was compared with numerical results for X sections.

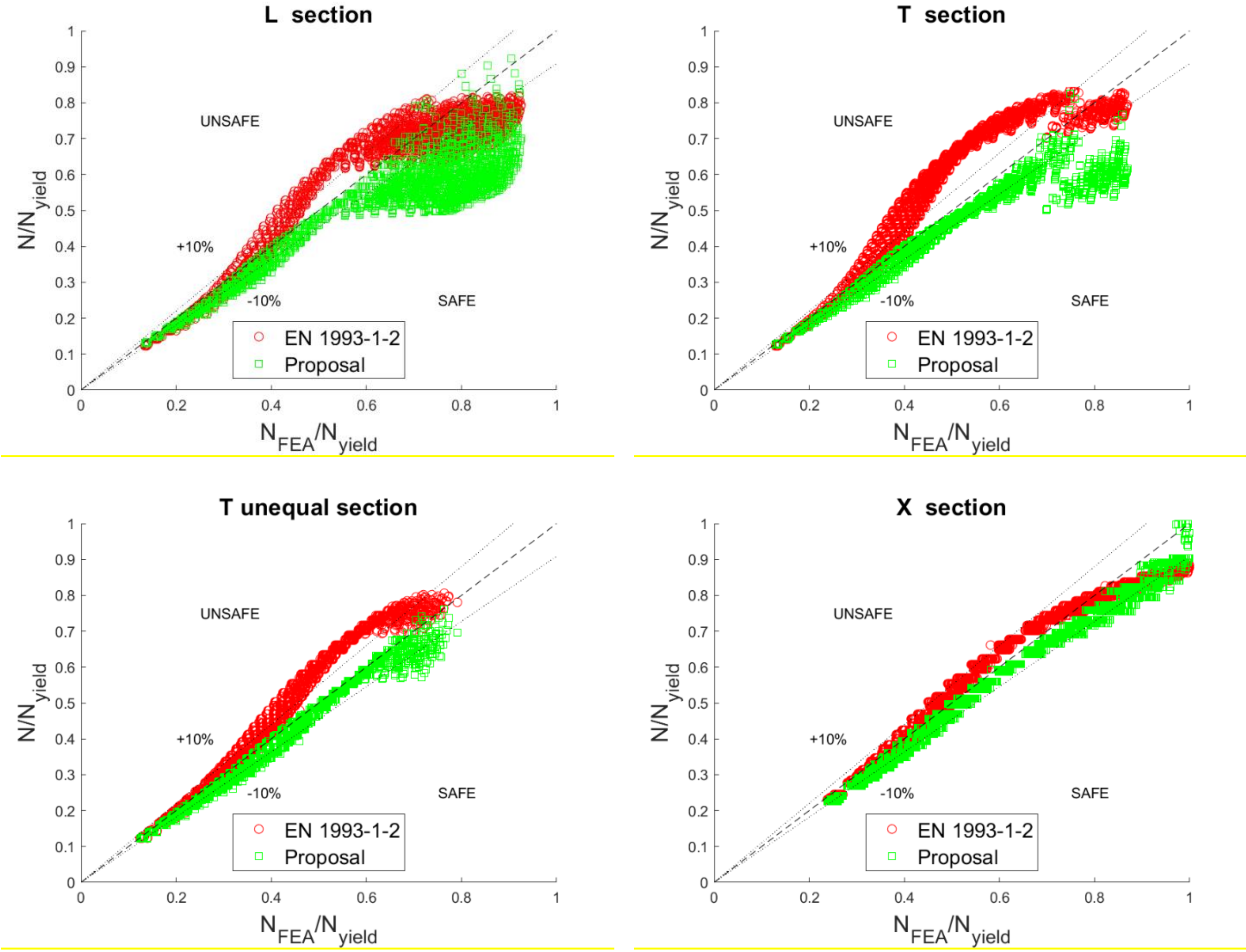

Fig. 7. Numerical results vs. design curves predictions

The outcomes of statistical investigation are depicted in Figure 8 in the form of cumulative normal distributions. The vertical line at $N/N_{FEA} = 1$ represents the safe-unsafe limit. The new model has lower standard deviations and significantly higher probabilities of safe predictions with respect to the ones from the actual design curves. Values higher than 91% were obtained at the safe-unsafe limit for all the sections and when a safety margin of 5% was included, the values were increased to about 98%.

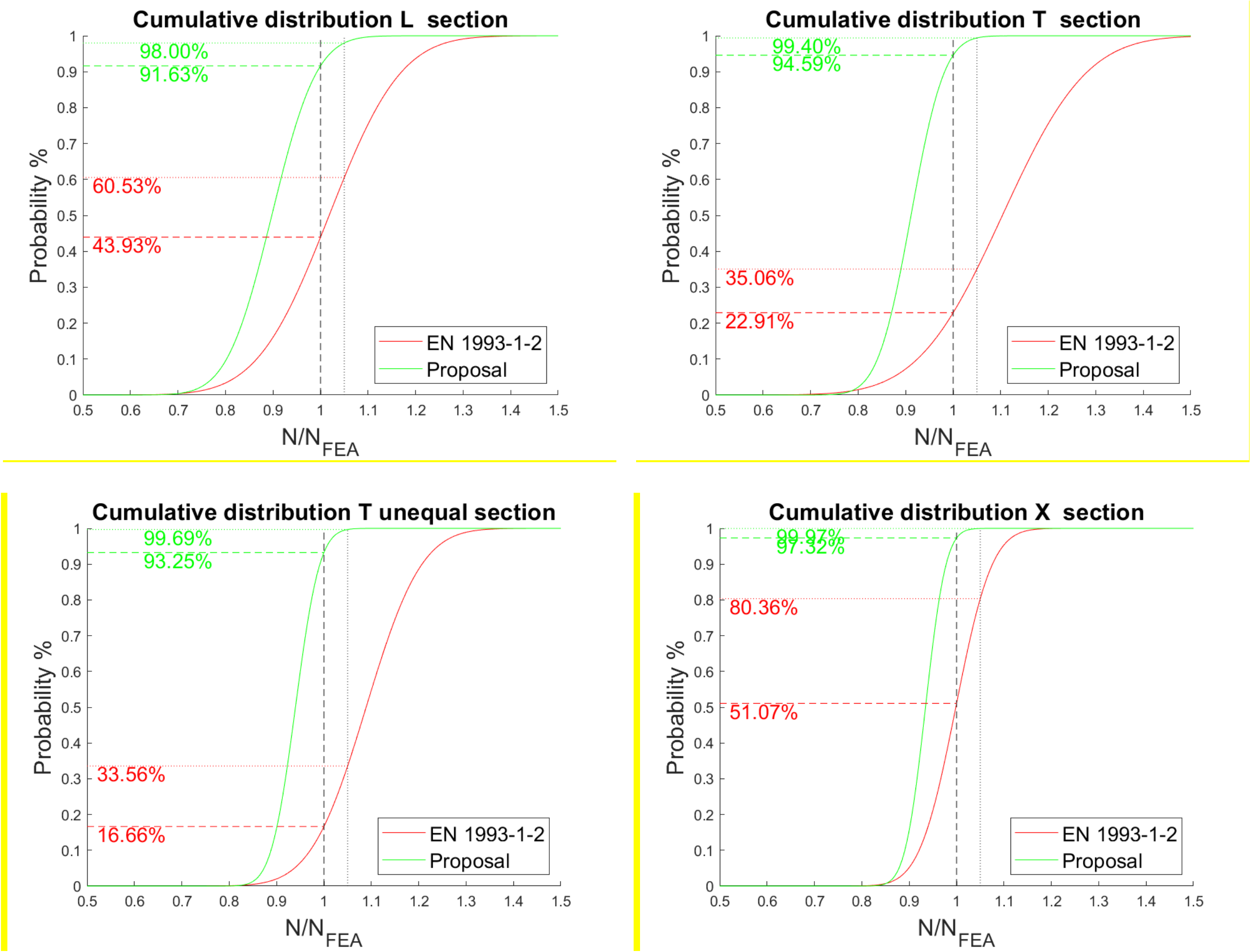

Fig. 8. Cumulative normal distributions

As previously stated, the numerical outcomes are influenced by the parameter B/t. While for $\bar{\lambda}_\theta \geq 0.7$ the depth-to-thickness ratio of the plates has no significant influence on the results, for $0.25 \leq \bar{\lambda}_\theta < 0.7$ numerical results are more spread (Figure 5) and in particular for L sections. Numerical observations for slenderness $0.25 \leq \bar{\lambda}_\theta < 0.7$ are associated with the region of scattered data in Figure 7. The introduction in the model of terms related to the B/t ratio could improve the fit of the numerical results and condense the cloud of data. However, for sake of simplicity, the authors preferred to neglect the influence of the B/t ratio. The statistical and safety investigations proved the proposed formulation to be sufficiently accurate and safe. Predictions are never safer than 40%, which is consistent with results obtained for design curves proposed for other instability phenomena at elevated temperatures [14, 34].

4.2. Slenderness modification

Although the predictions from the proposed model are considered safe and sufficiently accurate, an improved buckling curve can be obtained by introducing a modification in the definition of the slenderness. As stated by Taras and Greiner in [26], the length of the column l is not well represented by the non-dimensional slenderness $\bar{\lambda}_{cr}$ associated with the relevant buckling mode (i.e. torsional or flexural-torsional mode). A better representation of the length range is obtained by replacing the critical buckling load N_{cr} in Eq. (9) with the lowest flexural buckling load $\min\left(N_{cr,y}, N_{cr,z}\right)$

$$\bar{\lambda} = \bar{\lambda}_{cr,F} = \sqrt{\frac{Af_y}{N_{cr,F}}} = \sqrt{\frac{Af_y}{\min\left(N_{cr,y}, N_{cr,z}\right)}} \tag{14}$$

A similar observation was taken for cold-formed steel members at ambient temperature by Popovic et al. [19], who recommended to determine the slenderness for the proposed design buckling curve based on the flexural buckling strength about the minor axis. Consistently with this idea, in Figure 9 the numerical results are presented with respect to the non-dimensional slenderness at elevated temperature $\bar{\lambda}_\theta$ defined according to equations (8) and (14).

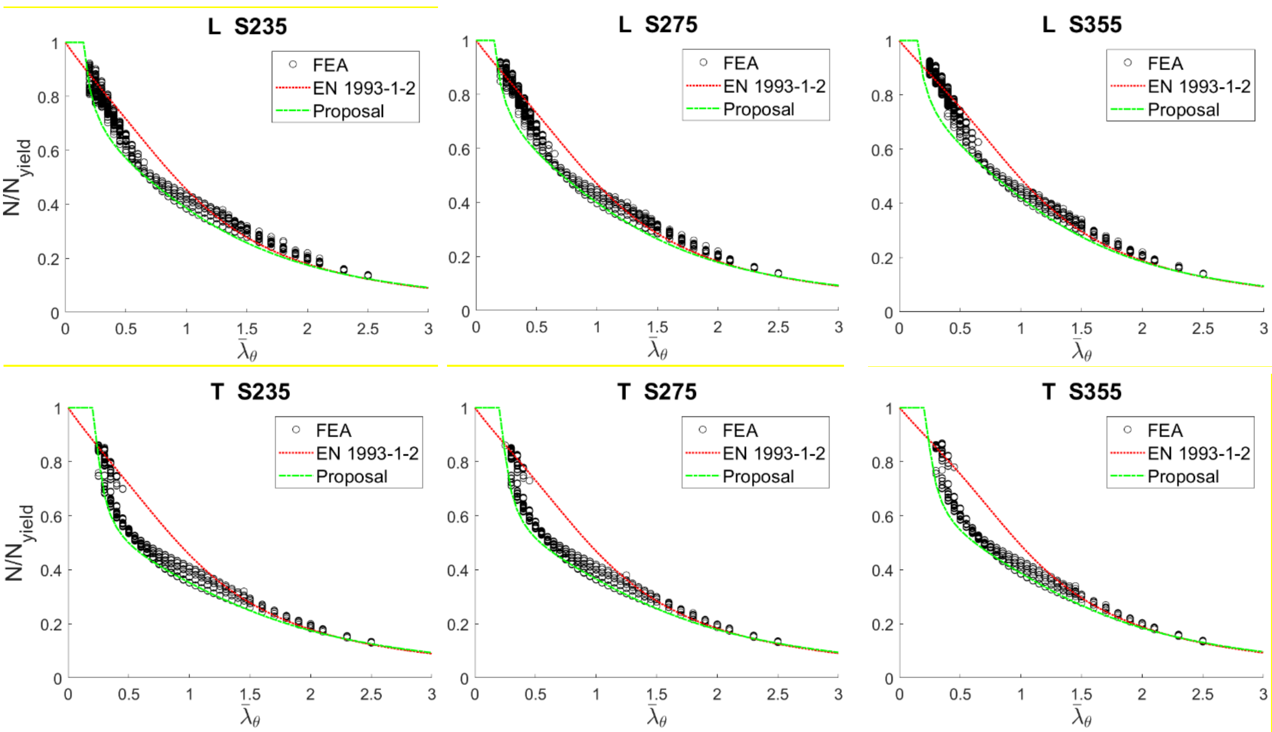

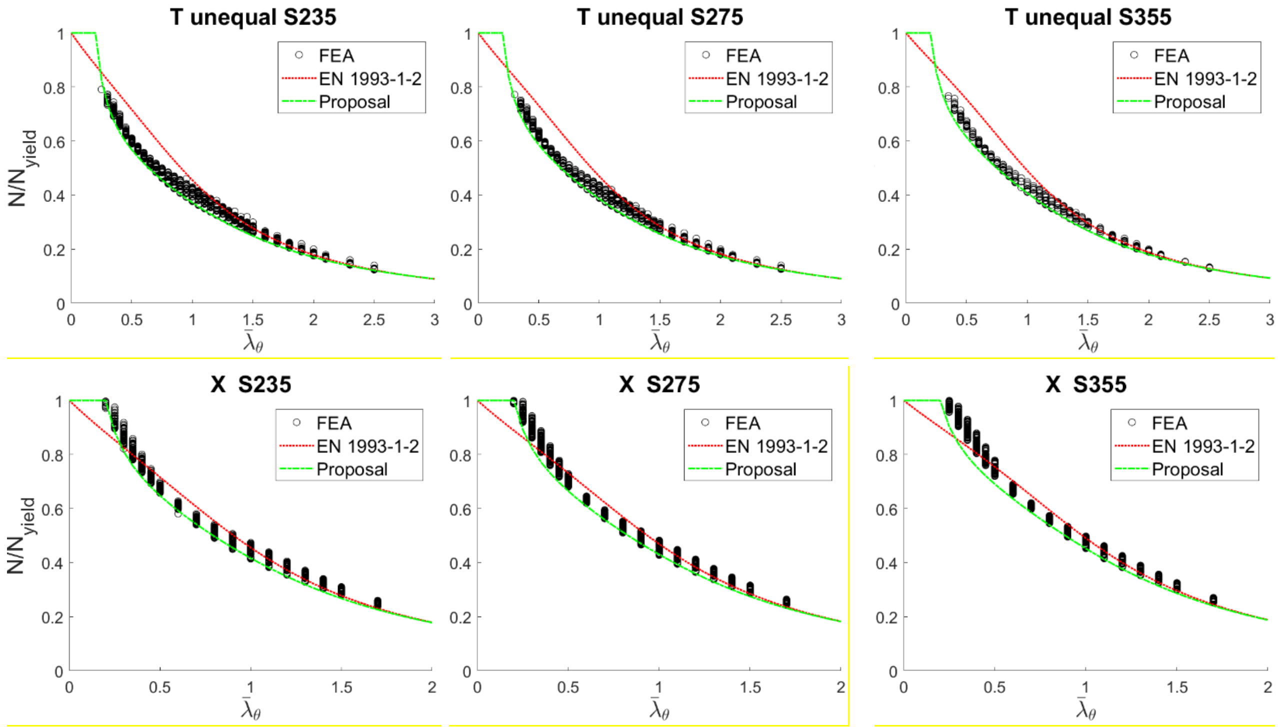

Fig. 9. Buckling curves for S235, S275 and S355 – $\bar{\lambda}_\theta$ = flexural slenderness

In this new configuration, the numerical results associated with stocky columns are less scattered compared to Figure 5, facilitating the fit by means of buckling curves. The actual and the proposed design curves evaluated according to the new slenderness definition are also given in Figure 9. The framework described in Section 4 was employed for the buckling curve proposal, but new parameters were defined in Table 5. As the X sections were almost exclusively subjected to flexural buckling, the same parameters were used.

Table 5. Parameter values for the proposed buckling curve – slenderness modification

	L	T	T (unequal)	X
β	1.00	1.25	1.10	0.85
γ	0.50	0.80	0.50	0.35
$\bar{\lambda}_0$	0.15	0.22	0.20	0.20

Failure loads from numerical simulation and from design curves are compared for the different cross-section types in Figure 10. Significantly improved predictions were obtained, as the range of underestimated values was reduced for the L and T sections. The model is still safe, as proved also by statistical investigation (Figure 11). Assuming a normal distribution, the probability of safe predictions was more than 96% for all the sections, while more than 99% of the values were safe when a safety margin of 1.05 was considered.

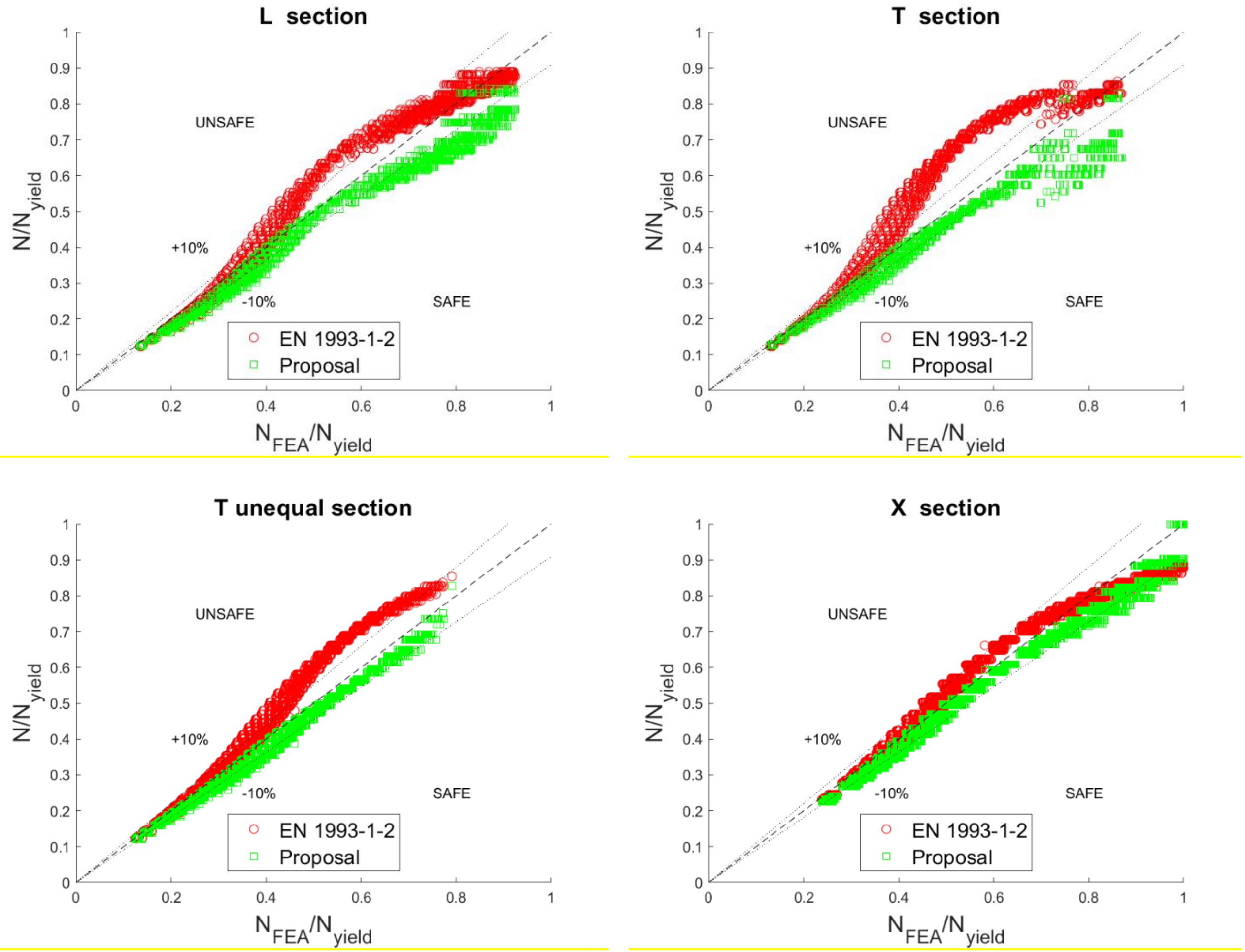

Fig. 10. Numerical results vs. design curves predictions – $\bar{\lambda}_{\theta}$ = flexural slenderness

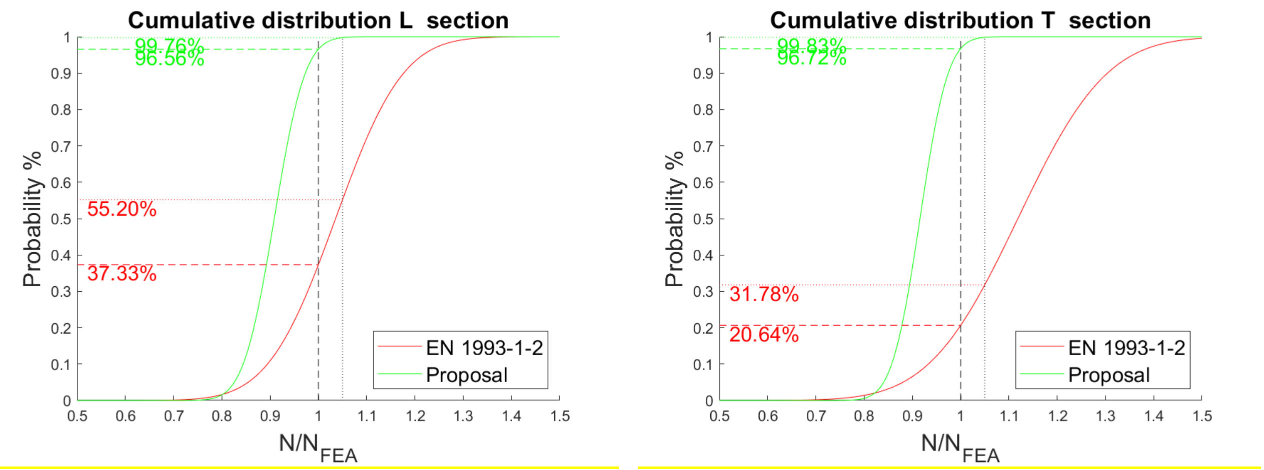

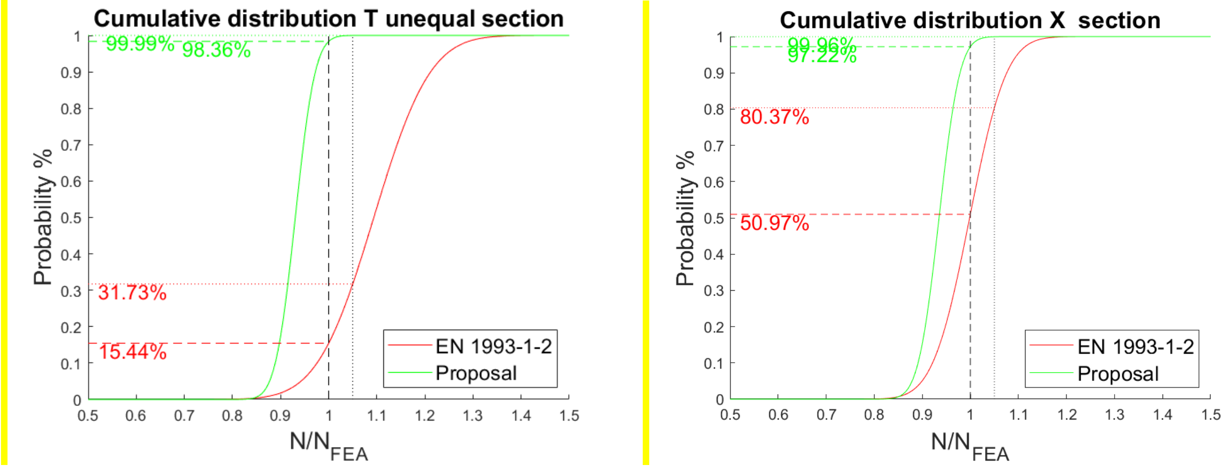

Fig. 11. Cumulative normal distributions– $\bar{\lambda}_{\theta}$ = flexural slenderness

In conclusion, according to the results, the model based on the flexural slenderness is more accurate and should be preferred.

5. Conclusions

This paper investigates the resistance at elevated temperature of compressed steel L profiles or closely spaced built-up members, whose load bearing capacity may be affected by torsional or flexural-torsional buckling. Though these members are widely used in the design practice, the EN 1993-1-2 provisions do not provide guidance and very few fundamental studies can be found in literature. Indeed, research works have mainly focused on flexural and flexural-torsional behaviour of cold-formed steel members and rarely at elevated temperatures, while such a behaviour in the fire situation of hot-rolled or welded profiles was not investigated. Thus, in the present work, a comprehensive numerical analysis of the buckling resistance of concentrically compressed L, T and X sections at elevated temperature was performed. In this respect, parametric analysis that relied on more than 23500 columns with cross sections classified as Class 1 to Class 3 was carried out for a range of critical temperatures, relevant in the design practice, between 400°C and 800°C. It was found that the actual EN 1993-1-2 provisions can lead to both conservative and unconservative predictions depending on the slenderness at elevated temperature $\bar{\lambda}_{\theta}$. In detail, for slenderness range of practical interest $0.5 \leq \bar{\lambda}_{\theta} < 1.5$ the EN 1993-1-2 buckling curve overestimates the load-bearing capacity. Thus, a new buckling curve as a function of the slenderness at elevated temperature $\bar{\lambda}_\theta$ and depending upon the cross-section shape and steel grade was proposed for concentrically compressed steel L, T and X members prone to torsional and flexural-torsional buckling. The proposed buckling curve is based on the general formulation provided in EN 1993-1-1 and EN 1993-1-2 and was calibrated by defining three parameters, namely β, γ and $\bar{\lambda}_\theta$, that differ upon the cross-section shape. The effect of the temperature on the results is small and despite the fact the effect of the B/t ratio is more evident for $\bar{\lambda}_\theta < 0.7$, it was decided to propose one simple model of buckling curve that provides safe and reasonable accurate predictions. Indeed, statistical investigation proved the proposal to be reliable and safe. In general, better statistical correlation was found between the finite element analysis (GMNIA) results and the proposed buckling curve rather than the EN 1993-1-2 buckling curve. Assuming normal distribution, probabilities of safe predictions higher than 91% were reached when the results were expressed in terms of the slenderness associated with the relevant buckling mode, whereas more than 96% of safe predictions were observed when the flexural slenderness was instead employed to better consider the effect of the member length. Indeed, the predictions in terms of the flexural slenderness are more accurate and its use is preferable. In conclusion, the proposed buckling curve allows for better predictions of the resistance of concentrically compressed L, T and X members in fire prone to torsional or flexural-torsional buckling. It is valid in the temperature range 400°C-800°C and for Class 1 to Class 3 cross-sections, while it does not consider the influence of local buckling typical of Class 4 cross-sections. Further investigations could be performed, for instance by employing more refined finite element models to account for the influence of connecting plates or battens. Finally, since the proposal is based on numerical analyses as no experimental tests on the investigated profiles are available in literature, future experimental campaign would be beneficial to confirm the proposal effectiveness.

Acknowledgements

The authors acknowledge funding from the Italian Ministry of Education, University and Research (MIUR) in the frame of the Departments of Excellence Initiative 2018–2022 attributed to DICAM of the University of Trento.

References

1. European Comitee for Standardisation (2005). *Eurocode 3 Design of steel structures - Part 1-1: General rules and rules for buildings*
2. European Comitee for Standardisation (2005). *Eurocode 3 Design of steel structures - Part 1-2: General rules - Structural fire design*
3. J.-M. Franssen, J.-B. Schleich, L.-G. Cajot (1995). *A simple Model for the Fire Resistance of Axially-loaded Members According to Eurocode 3*. Journal of Constructional Steel Research, Vol 35, pp. 49-69
4. J.-M. Franssen, J.-B. Schleich, L.-G. Cajot, W. Azpiazu (1996). *A simple Model for the Fire Resistance of Axially-loaded Members – Comparison with Experimental Results*. J. Construct. Steel Res, Vol 35, No. 3, pp. 175-204
5. C.G. Bailey, I. W. Burgess, R. J. Plank (1996). *The Lateral-torsional Buckling of Unrestrained Steel Beams in Fire.* J. Construct. Steel Res., Vol.36, No. 2, pp. 101-119
6. P. Vila Real e J.-M. Franssen (2000), *Lateral Torsional Buckling of Steel -Beams in Case of Fire – Numerical Modelling.* First International Workshop Structures in Fire, Copenhagen.
7. P. Vila Real e J.-M. Franssen (2001), *Numerical modelling of lateral buckling of steel I beams under fire conditions—comparison with Eurocode 3.* Journal of Fire Protection Engineering, Vol. 11, No. 2, pp. 112–128
8. P. Vila Real, P. A. G. Piloto, e J.-M. Franssen (2003). *A new proposal of a simple model for the lateral-torsional buckling of unrestrained steel I-beams in case of fire: experimental and numerical validation*. J. Constr. Steel Res., Vol. 59, No. 2, pp. 179–199
9. P. Vila Real, N. Lopes, L. S. da Silva, e J.-M. Franssen (2007). *Parametric analysis of the lateral–torsional buckling resistance of steel beams in case of fire*. Fire Saf. J., Vol. 42, No. 6–7, pp. 416–424

10. P. Vila Real, N. Lopes, L. S. da Silva, e J.-M. Franssen (2004), *Lateral-torsional buckling of unrestrained steel beams under fire conditions: improvement of EC3 proposal*. Comput. Struct., Vol. 82, No. 20, pp. 1737–1744
11. P. Vila Real, R. Cazeli, L. S. da Silva, A. Santiago, e P. Piloto (2004), *The effect of residual stresses in the lateral-torsional buckling of steel I-beams at elevated temperature*. J. Constr. Steel Res., Vol. 60, No. 3–5, pp. 783–793.
12. C. Couto, P. Vila Real, N. Lopes, B. Zhao (2016), *Numerical investigation of the lateral-torsional buckling of beams with slender cross section for the case of fire*. Engineering Structures, Vol. 106, pp. 410-421.
13. C. Couto, P. Vila Real, N. Lopes, B. Zhao (2016), *Local buckling in laterally restrained steel beam-columns in case of fire*. J. Construct. Steel Res., Vol. 122, pp. 543-556.
14. C. Couto, E. Maia, P. Vila Real, N. Lopes (2018), *The effect of non-uniform bending on the lateral stability of steel beams with slender cross-section at elevated temperatures*. Engineering Structures, Vol. 163, pp. 153-156.
15. J.-M. Franssen, F. Morente, P. Vila Real, F. Wald, A. Sanzel, B. Zhao (2016). *Fire Design of Steel Members with Welded or Hot-rolled Class 4 Cross-sections (FIDESC4)*
16. N. Silvestre, P. B. Dinis, D. Camotim (2013). *Developments on the Design of Cold-Formed Steel Angels*. J. Struct. Steel Res, Vol 139, No. 5, pp. 680-694
17. B. W. Schafer (2008). *Review: The Direct Strength Method of cold-formed steel member design*. J. Construct. Steel Res, Vol 64, pp. 766-778
18. G. M. De Barros Chodraui, Y. Shifferaw, M. Malite, B.W. Schafer (2007). *On the stability of cold-formed steel angles under compression*. Revista Escola de Minas, Vol 60, No. 2, pp. 355-363
19. D. Popovic, G. J. Hancock, K. J. R. Rasmussen (2001). *Compression tests on cold-formed angles loaded parallel with a leg*. J. Sruct. Steel Res, Vol 127, No. 6, pp. 600-607
20. T. Ranawaka, M. Mahendran (2010). *Numerical modelling of light gauge cold-formed steel compression members subjected to distortional buckling at elevated temperatures*. Thin-Walled Structures, Vol 48, No. 4-5, pp. 334-344

21. L. Laim, J. P. C. Rodrigues (2018). *Fire design methodologies for cold-formed steel beams made with open and closed cross-sections*. Engineering Structures, Vol. 171, pp. 759-778

22. P. B. Dinis, D. Camotim, N. Silvestre (2010). *On the local and global buckling behavior of angle, T-section and cruciform thin-walled members*, Thin-Walled Structures, Vol 48, pp. 786-797

23. R. Dabrowski (1988). *On Torsional Stability of Cruciform Columns*, J. Constr. Steel Res., Vol. 9, pp. 51-59

24. G. Chen, N. S. Trahir (2006). *Inelastic torsional buckling strengths of cruciform columns*, Engineering Structures, Vol. 16, No. 2, pp. 83-90.

25. N. S. Trahir (2012). *Strength design of cruciform steel columns.* Engineering Structures, Vol. 35, pp. 307-313.

26. A. Taras, R. Greiner (2007). *Torsional and flexural torsional buckling – A study on laterally restrained I-sections*, J. Constr. Steel Res. Vol. 64, pp. 725-731

27. J. C. Chapman, D. Buhagiar (1993). *Application of Young's buckling equation to design against torsional buckling.* Proceedings of the Institution of Civil Engineers: Structures and Buildings, Vol. 99, pp. 359-369.

28. J. Szalai, F. Papp (2010). *On the theoretical background of the generalization of Ayrton-Penny type resistance formulas,* J. Constr. Steel Res. Vol. 66, pp. 670-679

29. L. Possidente, N. Tondini, J.-M. Battini (2020). *3D Beam Element for the Analysis of Torsional Problems of Steel-Structures in Fire*. J. Struct. Eng., 146:(7), 10.1061/(ASCE)ST.1943-541X.0002665.

30. L. Possidente, N. Tondini, J.-M. Battini (2019). *Branch-switching procedure for post-buckling analyses of thin-walled steel members in fire*. Thin-Walled Structures, Vol 136, pp. 90-98

31. S. P. Timoshenko, J. M. Gere (1963). *Theory of elastic stability*. McGraw-Hill, New-York

32. N. S. Trahir (1993). *Flexural-Torsional Buckling of Structures*. E & FN Spon, London.

33. S. E. Quiel, M. E. M. Garlock (2010), *Calculating the buckling strength of steel plates exposed to fire*. Thin-Walled Structures., Vol. 48, No. 9, pp. 684-695

34. C. Couto, P. Vila Real, N. Lopes, B. Zhao (2015), *Resistance of steel cross-sections with local buckling at elevated temperatures*. J. Construct. Steel Res., Vol. 109, pp. 101-114

35. C. Couto, P. Vila Real, N. Lopes, B. Zhao (2014), *Effective width method to account for the local buckling of steel thin plates at elevated temperatures*. Thin-Walled Structures., Vol. 84, pp. 134-149

36. J. Jönsson, T.-C. Stan (2017), European column buckling curves and finite element modelling including high strength steels. J. Construct. Steel Res., Vol 128, pp. 136-151

37. J.M. Franssen, T. Gernay (2017). *Modeling structures in fire with SAFIR®: Theoretical background and capabilities.* Journal of Structural Fire Engineering, Vol. 8, No. 3, pp. 300-323

38. L.M. Gil-Martín, E. Hernández-Montes (2019). *Principal Sectorial Coordinates System*. Archive of Applied Mechanics.

39. Vlasov, V.Z. (1961). *Thin Walled Elastic Beams*. Israel Program for Scientific Translations. Jerusalem